Scientific paper

Fiber-Bridging Constitutive Law of Engineered Cementitious Composites

En-Hua Yang[1], Shuxin Wang[1], Yingzi Yang[2] and Victor C. Li[3]

Received 2 July 2007, accepted 31 October 2007

Abstract

This paper is on modeling and measuring fiber-bridging constitutive law of Engineered Cementitious Composites (ECC), a high performance fiber-reinforced cementitious composite featuring high tensile ductility. Fiber-bridging constitutive law plays an important role in the multiple cracking behavior of ECC. Therefore, proper control of fiber-bridging behavior through tailoring material microstructure is the key to successfully designing tensile strain-hardening ECC. In this paper, an analytical fiber-bridging model of ECC which connects material constituent parameters and composite properties, built on a previous simplified version, was proposed. To improve accuracy of crack opening prediction, new mechanisms of fiber/matrix interactions, specifically fiber two-way debonding and pull-out, matrix micro-spalling, and Cook-Gordon effects were included. This revised model was compared with experimental measurement of fiber-bridging behavior and the validity of the model was confirmed. It is expected that this model will greatly improve ECC design technology in terms of steady-state crack width control, key for structural long-term durability, and in terms of composite tensile properties important for structural safety at ultimate limit state.

1. Introduction

Engineered Cementitious Composites (ECC) represents a special kind of high performance fiber-reinforced cementitious composites featuring high tensile ductility. Unlike concrete and conventional fiber-reinforced concrete (FRC) which show unloading after matrix first cracking (tension softening), ECC exhibits tensile strain-hardening behavior achieved by sequential development of matrix multiple cracking. **Figure 1** gives the typical tensile stress-strain-crack width curve of an ECC containing 2 vol.% polyvinyl alcohol (PVA) fiber.

As can be seen, the tensile ductility of ECC is several hundred times that of normal concrete and crack width in ECC is self-controlled and reaches a constant value (~ 60 μm) after 1% elongation. The fracture toughness of ECC is similar to that of aluminum alloy (Maalej *et al*. 1995) and ECC remains ductile even when subjected to high shear stress (Li *et al*. 1994). High tensile ductility and toughness of ECC material greatly elevates the mechanical performance of reinforced ECC (R/ECC) structure by preventing brittle failure and loss of structural integrity which is usually found in traditional reinforced concrete (R/C) structure under excessive loading. In fact, it has been demonstrated experimentally that R/ECC structural members surpass normal R/C structural members in structural load carrying capacity, deformability, and energy absorption capacity under monotonic (Li and Wang 2002), reverse cyclic (Fischer and Li 2002, Fukuyama *et al*, 1999), and impact (Zhang *et al*. 2005) loading.

In addition, high ductility and tight crack width of ECC are expected to improve the durability of infrastructure in three ways. First, the magnitude of crack width controls various transport properties in cracked concrete materials and has a direct impact on durability (Lepech and Li 2005a). It has been reported that ECC has lower water permeability (Lepech and Li 2005b) and lower effective chloride diffusivity (Miyazato and Hiraishi 2005; Sahmaran *et al*. 2006) in the presence of microcracks when compared with cracked concrete in

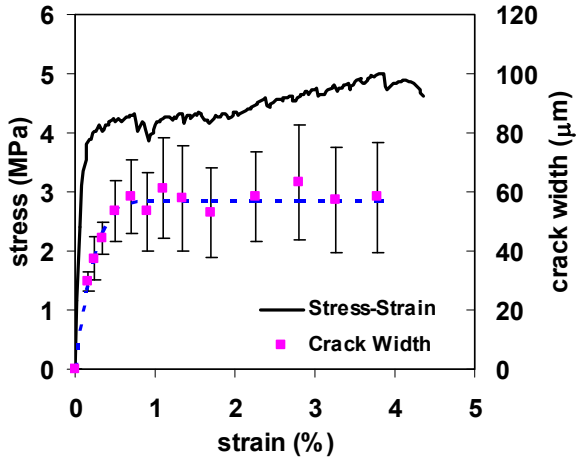

Fig. 1 Typical tensile stress-strain-crack width relationship of PVA-ECC (mix 45).

[1]Research Assistant, Department of Civil and Environmental Engineering, University of Michigan, Ann Arbor, Michigan, USA.
[2]Associate Professor, Department of Civil Engineering, Harbin Institute of Technology, Harbin, China.
[3]Professor, Department of Civil and Environmental Engineering, University of Michigan, Ann Arbor, USA. *E-mail*:vcli@umich.edu

which the crack width is not self-controlled and is usually in the range of several hundred micrometer to several millimeter. Second, self-healing of cracked ECC has been observed due to the tight crack width in ECC (Yang *et al*. 2005; Li and Yang, 2007). Third, even if the first two mechanisms fail and corrosion occurs, ECC material ductility is likely to prevent corrosion introduced spalling as a secondary protection (Li and Stang 2004). These observations suggest that steel reinforced concrete structures will most likely have better durability when ECC with self-controlled tight crack width is used in place of normal concrete.

The ingredients of ECC are similar to that of normal FRC, except for the absence of coarse aggregates. While various fiber types have been used in the past, ECC reinforced with PVA fibers (PVA-ECC) has attractive characteristics in terms of cost, processing, mechanical properties, and durability and represents the most practical ECC for field application to date. Notably, PVA-ECC utilizes short, randomly distributed fibers with a moderate volume fraction (2% or less in general). With this relatively small amount of short fibers, self-consolidating PVA-ECC (Kong *et al*. 2003; Fischer *et al*, 2003) has been designed for use with regular construction equipment (Li *et al*. 2005). The high performance, moderate fiber content combination is attained by micromechanics-based composites optimization (Li 1997; Lin and Li 1997). Micromechanics provides guidance in specific selection and tailoring of the type, size and amount of ingredients. As a result, the fiber, matrix and interface interacts synergistically to produce controlled multiple microcracking when overloaded in tension, while suppressing the localized fracture mode commonly observed in FRC. PVA-ECC is currently emerging in full scale structural applications in Japan (Kunieda and Rokugo 2006) and in the United States (Michigan_DOT 2005).

Fiber-bridging constitutive law $\sigma(\delta)$ describes the relationship between the bridging stress σ transferred across a crack and the opening of this crack δ. In the development of ECC, $\sigma(\delta)$ relationship is of primary importance. It relates to material microstructure (micro-scale) on one hand, and governs composite tensile strain-hardening behavior (macro-scale) on the other. Therefore, control of $\sigma(\delta)$ curve through tailoring material microstructure is the key to successfully design ECC material properties in general, and tensile properties, i.e. tensile strain capacity and ultimate tensile strength, and steady-state crack width in particular. The tensile properties of ECC are important to the structural safety at ultimate limit state as the steady-state crack width is to the structural long-term durability.

This paper aims at establishing an analytical fiber-bridging model of ECC, built on a previous simplified version (Lin *et al*. 1999). To improve accuracy of crack opening prediction, new mechanisms of fiber/matrix interactions, specifically fiber two-way debonding and pull-out, matrix micro-spalling, and Cook-Gordon effects are included. It is expected that this improved $\sigma(\delta)$ model will greatly benefit future ECC material design technology in terms of steady-state crack width control which is the key for structural long-term durability and composite tensile properties which is important for structural safety at ultimate limit state. In the following section, the role of $\sigma(\delta)$ curve in controlling ECC tensile strain-hardening behavior is introduced first. A fiber-bridging model for ECC is then proposed. To verify the fidelity of the revised fiber-bridging model, $\sigma(\delta)$ curve was determined experimentally for comparison with the predicted $\sigma(\delta)$ relationship.

2. Strain-hardening criteria

The pseudo strain-hardening behavior in ECC is a result of sequential development of matrix multiple cracking. A fundamental requirement for this multiple cracking behavior is that steady-state cracking occurs under tension, i.e. a flat crack can form after initiating from a defect site and extends indefinitely through the matrix (Wang and Li 2006). In this condition, the ambient loading and the crack opening remain constant and bridging fibers sustain and pass the load without rupturing and diminishing. Further loading initiates another microcrack from another defect site and subsequent flat crack propagation. Repeated formation of such steady-state cracks results in multiple cracking and strain-hardening as depicted in **Fig. 1**.

The condition for steady-state flat crack *propagation* was analyzed by Marshall and Cox (1988) using J-integral method. When fiber-bridging behavior is characterized by the $\sigma(\delta)$ relation, the condition can be expressed in the following form,

$$J_{tip} \le \sigma_0 \delta_0 - \int_0^{\delta_0} \sigma(\delta) d\delta \equiv J_b^{'} \tag{1}$$

i.e. the crack tip toughness J_{tip} must be limited to less than the complementary energy $J_b^{'}$ of the bridging fibers (springs) as defined by the right-hand-side of Eqn. (1). J_{tip} approaches the matrix toughness K_m^2/E_m at small fiber content, where K_m is the matrix fracture toughness and E_m is the matrix Young's Modulus. Eqn. (1) expresses the energy balance (energy supplied by external work and energy consumed by material break-down at the crack tip and subsequently opening of the springs near the crack tip) per unit crack advance during steady-state crack propagation. **Figure 2** schematically illustrates such energy balance concept, where $J_b^{'}$ and J_{tip} are represented by the hatched and shaded area respectively.

Prior to flat crack propagation, it is necessary for a microcrack to *initiate* (from a defect site) at a load level below the fiber-bridging capacity. This consideration translates into another condition for strain-hardening: that the matrix tensile cracking strength σ_c must not exceed the maximum fiber-bridging strength σ_0.

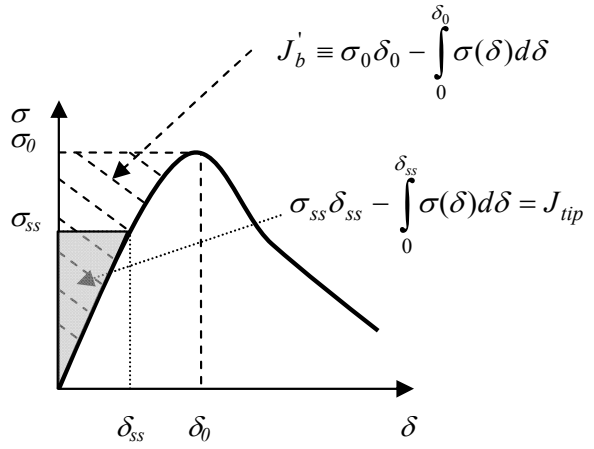

Fig. 2 Typical $\sigma(\delta)$ curve for tensile strain-hardening composite. Hatched area represents complimentary energy J_b'. Shaded area represents crack tip toughness J_{tip}.

$$\sigma_c < \sigma_0 \tag{2}$$

where σ_c is determined by the preexisting flaw size and the matrix fracture toughness K_m. While the energy criterion (Eqn. (1)) governs the crack propagation mode, the strength-based criterion represented by Eqn. (2) governs the initiation of cracks. Satisfaction of both Eqn. (1) and (2) is necessary to achieve ECC tensile strain-hardening behavior; otherwise, relatively poor tensile strain-capacity or even normal tension-softening FRC behavior results.

As can be seen, both criteria are related to fiber-bridging constitutive law. It determines the complementary energy J_b' in Eqn. (1) as well as the maximum bridging strength σ_0 in Eqn. (2). Therefore, the $\sigma(\delta)$ relationship critically controls the tensile strain-hardening behavior of ECC materials.

3. Fiber-bridging model

ECC is a cement-based composite and usually reinforced with short (6-12mm), randomly distributed small diameter (10-100μm) micro-fibers. The construction of fiber-bridging constitutive law starts from modeling a single fiber pullout behavior against the surrounding matrix. The $\sigma(\delta)$ relationship can then be obtained by averaging the contributions from fibers with different embedment length and orientation across the crack plane. Specific consideration is placed on ECC systems which exhibit two-way fiber debonding-pullout due to a slip-hardening interfacial bond. PVA-ECC belongs to this class. Finally, matrix micro-spalling as well as Cook-Gordon effect are considered to refine the model. Due to the absence of coarse aggregate in ECC mix design, aggregate bridging is not considered in the present study.

3.1 Modeling of single fiber behavior

When a fiber is subjected to a pullout force, it must first debond from the surrounding matrix before it can be pulled out. The debonding process may be viewed as crack propagation along the interface tunnel from near the matrix crack surface toward the embedded end. After debonding, the interface is purely governed by frictional force. Such tunneling crack problem was studied by Lin and Li (1997). Assuming constant frictional stress τ_0 and debonding fracture energy G_d (also referred to as chemical bond in this paper), during debonding stage (short-range relative sliding) the single fiber-bridging stress $\sigma_{debonding}$ versus the fiber displacement (at exit point) relative to the matrix crack surface u is given by

$$\sigma_{debonding} = 2\sqrt{(\tau_0 u + G_d)\frac{2E_f(1+\eta)}{d_f}} \tag{3}$$

where E_f and d_f are fiber Young's modulus and diameter, respectively, and η is a parameter expressing the ratio of the effective (accounting for volume fraction) fiber stiffness to effective matrix stiffness. η approaches to zero as the fiber content becomes small.

After debonding is completed, the fiber is in the pullout stage. For some types of fiber, particularly PVA fiber, significant slip-hardening response was observed during long-range pullout. Assuming the frictional stress is linear to the slip distance with coefficient β (referred as slip-hardening coefficient (Lin and Li 1997)), the fiber stress $\sigma_{pullout}$ during pullout stage can be expressed as

$$\sigma_{pullout} = \frac{\tau_0}{d_f}(L_e - u - \delta_c)\left(1 + \frac{\beta(u-\delta_c)}{d_f}\right) \tag{4}$$

$$\delta_c = \frac{2\tau_0 L_e^2(1+\eta)}{E_f d_f} + \sqrt{\frac{8G_d L_e^2(1+\eta)}{E_f d_f}} \tag{5}$$

where L_e is the fiber embedment length and δ_c corresponds to the displacement at which full-debonding is completed. A schematic illustration of single fiber pullout behavior is shown in **Fig. 3**. At the end of debonding, there is a sudden load drop due to unstable extension of the tunnel crack. Subsequently, the fiber is held back in the matrix only by frictional bonding. The magnitude of the drop can be used to calibrate the chemical bond G_d. During the debonding and pullout stages, the fiber may rupture if the load P exceeds the fiber tensile strength, which is often the case in PVA-ECC system due to strong slip-hardening effect (Redon *et al*. 2001).

In short fiber composite systems such as ECC, most fibers are oriented at an arbitrary angle ϕ relative to the crack plane ($\phi = 0$ when fiber is perpendicular to the plane and $\phi = \pi/2$ when fiber is parallel to the plane). Misaligned fibers are subjected to additional frictional stress due to the interaction with the matrix when the fiber exits the matrix. For flexible polymeric fiber, Mor-

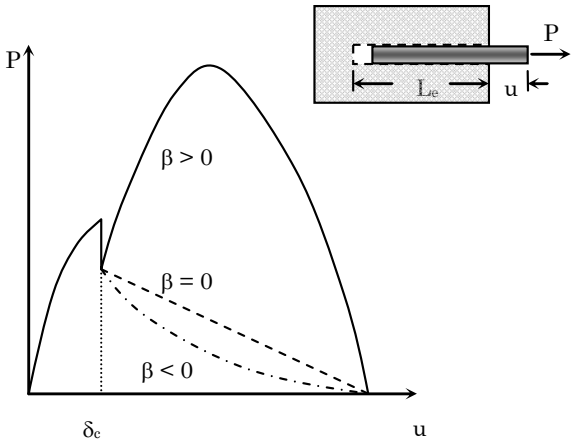

Fig. 3 Single fiber pullout behavior: (β > 0) slip-hardening; (β = 0) interface friction is independent of slip distance; and (β < 0) slip-softening.

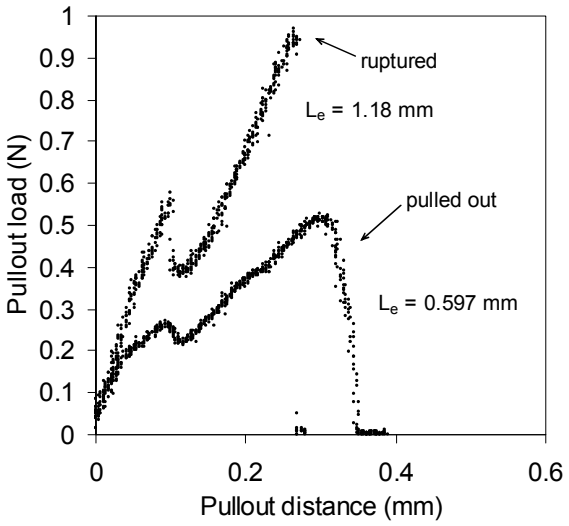

Fig. 4 Single fiber pullout curves of PVA-ECC M45 (fiber diameter 39 μm).

ton and Groves (1976) and Li *et al*. (1990) suggested the following empirical relation to account for the increase of bridging force P due to an inclination angle ϕ by making analogy to an Euler friction pulley at the fiber exit point,

$$P(\phi) = P(0)e^{f\phi} \tag{6}$$

where f > 0 is referred to as the snubbing coefficient.

Some types of fiber have strength which are vulnerable to bending and lateral stress. Macroscopically, these fibers exhibit strength reduction when loaded at an inclined angle to the crack plane. For PVA fiber, Kanda and Li (1998) introduced a strength reduction coefficient f' to account for this effect in the following form,

$$\sigma_{fu}(\phi) = \sigma_{fu}(0)e^{-f'\phi} \tag{7}$$

where σ_{fu} is the fiber rupture strength.

3.2 Two-way fiber pullout consideration

Many reinforcing fibers for cementitious composites, such as polyethylene fiber, polypropylene fiber, and smooth steel fiber, do not exhibit significant slip-hardening response, i.e. β approaches 0 or even goes negative (**Fig. 3**). Consequently, for bridging fibers, after complete debonding of the short embedment side, the long embedment side remains anchored since the load begins to drop. The increase of crack opening causes the short embedment side to be pulled out, and the elastic stretch of the long embedment side is negligible. The scenario; however, may be different in PVA fiber system, where strong slip-hardening behavior is present. Redon and Li (2001) suggested that slip-hardening of PVA fiber in a cement matrix was due to an abrasion and jamming effect during sliding of the fiber in the matrix tunnel. **Figure 4** shows typical responses of single PVA fiber pulled out from ECC mix 45 (M45) matrix. When the embedment length is small (e.g. L_e = 0.597 mm), the fiber can be pulled out from the matrix completely. When the embedment length is large (e.g. L_e = 1.18 mm), the fiber ruptures. The most significant observation however is that due to strong slip-hardening behavior the pullout load (after full debonding, first peak) can be much higher than the load at the completion of debonding. For PVA fibers bridging a crack, therefore, after the completion of debonding at short embedment side, the long embedment side may continue debonding and eventually enter the pullout stage such that two-way fiber pullout occurs. In this case, the contributions of slip displacement from both sides of the fiber across the crack to the total crack opening δ should be included. The possibility of two-way fiber debonding and pull-out was originally suggested by Wang *et al* (1988).

The modeling of two-way fiber pullout is illustrated in **Fig. 5**. For given crack opening δ, the contribution δ_L and δ_S from the long embedment segment (length L_L) and the short embedment segment (length L_S), respectively, can be calculated from the fiber load balance,

$$\delta = \delta_L + \delta_S \tag{8}$$

$$\delta_L = \delta_S \qquad \text{for } \delta < 2\delta_{0S} \tag{9}$$

$$P_d(\delta_L) = P_p(\delta_S, L_S) \qquad \text{for } \delta_S > \delta_{0S} \text{ and } \delta_L < \delta_{0L} \tag{10}$$

$$P_p(\delta_L, L_L) = P_p(\delta_S, L_S) \qquad \text{for } \delta_S > \delta_{0S} \text{ and } \delta_L > \delta_{0L} \tag{11}$$

The debonding load P_d and pullout load P_p are given by

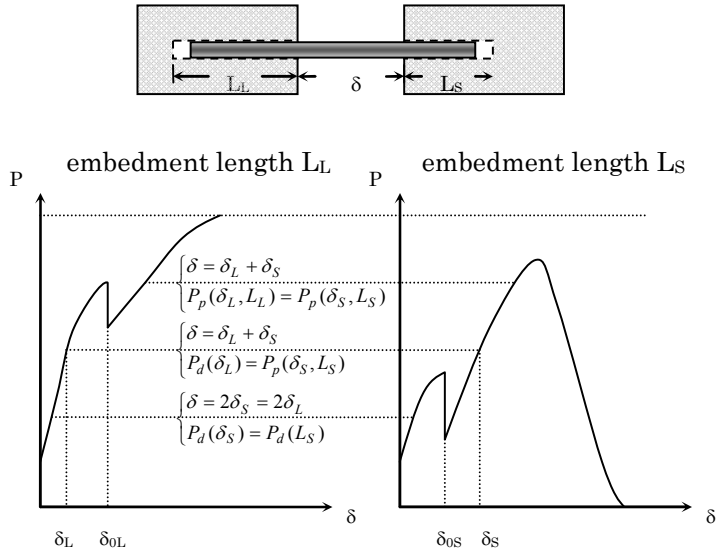

Fig. 5 Modeling of two-way pullout: (left) load vs. displacement curve of the long embedment side; (right) load vs. displacement curve of the short embedment side.

$$P_d(\delta) = \pi\sqrt{(\tau_0\delta + G_d)\frac{E_f d_f^3(1+\eta)}{2}} \tag{12}$$

$$P_p(\delta, L) = \pi\tau_0(L - \delta + \delta_0)(d_f + \beta(\delta - \delta_0)) \tag{13}$$

where δ_0 is the crack opening corresponding to complete debonding,

$$\delta_0(L) = \frac{2\tau_0 L^2(1+\eta)}{E_f d_f} + \sqrt{\frac{8G_d L^2(1+\eta)}{E_f d_f}} \tag{14}$$

$$\delta_{0L} = \delta_0(L_L) \tag{15}$$

$$\delta_{0S} = \delta_0(L_S) \tag{16}$$

3.3 Matrix micro-spalling consideration

Matrix micro-spalling at the fiber exit is commonly observed in random fiber reinforced brittle matrix composites, including PVA-ECC (Kanda and Li 1998). When the pullout force at the fiber exit is misaligned with the orientation of the embedded segment, stress concentration at the bearing point causes local failure of supporting matrix. The size of the spalled matrix piece is governed by the bearing force, which is a function of external load on the fiber, matrix strength, matrix stiffness, and inclination angle.

A semi-empirical equation for estimating the spalling size s is proposed as following,

$$s = \frac{P\sin\left(\frac{\phi}{2}\right)}{kd_f\sigma_m\cos^2\left(\frac{\phi}{2}\right)} \tag{17}$$

where P is the external force acting on the fiber; ϕ is the fiber inclination angle; σ_m is the matrix tensile strength, and k is the spalling coefficient (**Fig. 6**). k is a dimensionless constant related to fiber geometry and matrix stiffness, and can be calibrated by experimental observation. In this equation, the spalling size is assumed to be proportional to the external load on fiber exit and inversely proportional to matrix tensile strength and fiber diameter. The trigonometric terms reflect the force decomposition and geometric feature of the bearing portion of the matrix. An illustration of Eqn. (17), by plotting spalling size s against force P and inclination angle ϕ, is shown in **Fig. 6**. For typical forces in PVA fibers in ECC, the predicted spall size (for k = 500) is in the range of 0-28 μm, consistent with those observed experimentally.

Physically, matrix micro-spalling relieves stress concentration particularly on stretched bridging fibers. As illustrated in **Fig. 7**, spalling also changes the fiber inclination angle ϕ to a smaller ϕ'. Since the strength of PVA fiber degrades significantly at high inclination angle, the existence of matrix spalling serves to delay fiber rupture and allows larger crack opening as well as higher peak bridging stress.

Microscopic observation indicates that the spalling size s of PVA-ECC ranges from several micrometers to several tens of micrometers and is mostly limited by the fiber diameter. In PVA-ECC system, considering a typical steady-state crack width of 60 μm, the maximum elastic stretch of the fiber segments freed from spalling (i.e. total length 2s) will not exceed 2 μm at the peak load, which is negligible compared to the crack opening. Therefore, the elastic deformation of the fiber segments freed from spalling can be neglected without significant influence on the model accuracy. With this simplification, the modeling of single fiber-bridging behavior with

consideration of both two-way pullout and matrix spalling can be reduced to the problem of two-way pullout with a modified δ. As illustrated in **Fig. 7**, for a given crack opening δ,

$$\delta' = \sqrt{4s^2 + 4s\delta\cos\phi + \delta^2} \tag{18}$$

$$\phi' = \sin^{-1}\left(\frac{\delta\sin\phi}{\delta'}\right) \tag{19}$$

$$\delta_{eff} = \delta' - 2s \tag{20}$$

where δ_{eff} will replace δ in Eqn. (8) and s is given by Eqn. (17). Single fiber-bridging behavior P(δ) can then be obtained by evaluating Eqn. (8) – (20).

3.4 Averaging – modeling of fiber randomness

The randomness of fiber location and orientation is accounted for in the modeling of the σ(δ) relation by adopting probability density functions that describe the spatial variability of the fibers (Wang *et al*. 1990). Eqn. (21) shows the formulation of bridging stress σ versus crack opening δ relation. P(z, ϕ) is the bridging force contributed by a single fiber with centroidal distance z and orientation angle ϕ relative to the crack plane. p(z, ϕ) is the probability density function of fiber with distance z and orientation ϕ. A_f and V_f are the cross-sectional area and volume fraction of fiber, respectively.

$$\sigma(\delta) = \frac{1}{A_f V_f}\int P(z,\phi)p(z,\phi)dzd\phi \tag{21}$$

In general, the probability density functions of z and ϕ are independent of each other. For the case of 3-D uniform random distribution, p(z, ϕ) can be expressed as following:

$$p(z,\phi) = p(z)p(\phi) \tag{22}$$

$$p(z) = \frac{1}{l_f} \qquad -\frac{l_f}{2} \le z \le \frac{l_f}{2} \tag{23}$$

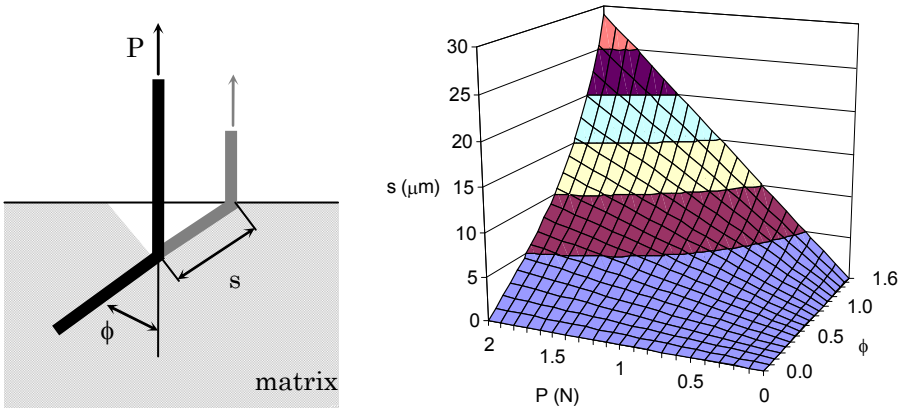

Fig. 6 Dependence of matrix spalling size s on inclination angle ϕ and fiber load P (Eqn. (17), assuming matrix tensile strength σ_m = 5 MPa, fiber diameter d_f = 39 μm, and spalling coefficient k = 500).

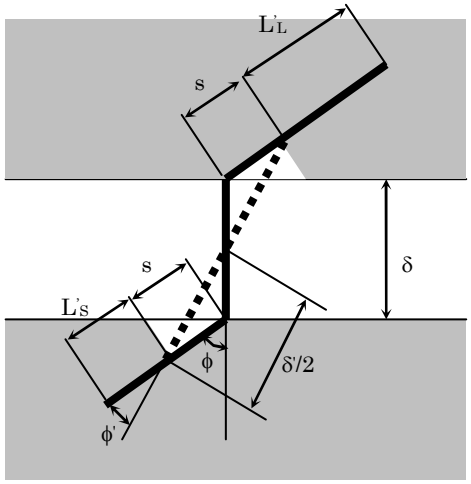

Fig. 7 Schematic of inclined bridging with matrix spalling.

$$p(\phi) = \sin(\phi) \qquad 0 \le \phi \le \frac{\pi}{2} \tag{24}$$

The random distribution assumption is generally valid in ECC materials, where short fiber and low fiber volume fraction, typically no more than 2%, are adopted. Mix rheology of ECC is also engineered such that uniform fiber distribution is readily achievable without clustering. The fiber orientation however may be constrained, for instance in spray process where ECC is applied layer by layer. In the case of 2-D random distribution, the orientation probability of fiber can be expressed as

$$p(\phi) = \frac{2}{\pi} \qquad 0 \le \phi \le \frac{\pi}{2} \tag{25}$$

The composite fiber-bridging behavior $\sigma(\delta)$ relation is available through averaging of all fiber force on the crack plane, as defined by Eqn. (21). In this study, Eqn. (21) and Eqn. (8) – (20) are numerically evaluated. Small increment in δ was chosen to ensure accuracy.

3.5 Cook-gordon effect

Another mechanism which contributes to additional compliance in the $\sigma(\delta)$ curve is the Cook-Gordon effect. Cook-Gordon effect describes a premature fiber/matrix interface debonding normal to the fiber axis caused by a tensile stress located ahead of a blunt matrix crack propagating towards a fiber under remote tensile load as depicted in **Fig. 8(a)**. Therefore, fiber debonding takes place ahead of the matrix crack, resulting in stretching of a free fiber segment α (Cook-Gordon parameter) and additional crack opening δ_{cg} as shown in **Fig. 8(b)**. Li *et al*. (1993) assumed that this phenomenon applies to all fibers regardless of orientation, so that δ_{cg} can be directly computed from the bridging force P. For a single fiber, the additional displacement may be estimated as follows,

$$\delta_{cg} = \frac{4\alpha P}{\pi d_f^2 E_f} \tag{26}$$

Noting that when P is independent of ϕ and z, the integration of Eqn. (21) gives the number of fibers bridging across the crack per unit area times P.

$$\sigma = P\frac{A_f}{V_f}\int p(z,\phi)dzd\phi \equiv PN_B \tag{27}$$

where N_B is the number of fiber-bridging across the crack per unit area and can be defined as

$$N_B = \frac{A_f}{V_f}\int p(z,\phi)dzd\phi = \frac{A_f}{V_f}\eta_B \tag{28}$$

where

$$\eta_B \equiv \int p(z,\phi)dzd\phi \tag{29}$$

defines the efficiency of bridging in terms of the amount of fibers bridging across a crack with respect to orientation effect. The P – δ_{cg} relationship for a single fiber, Eqn. (26), may be substituted into Eqn. (21). That is:

$$\delta_{cg} = \frac{\alpha\sigma}{V_f E_f \eta_B} \tag{30}$$

so that the total crack opening δ_{tot} is approximately given as

$$\delta_{tot} = \delta + \delta_{cg} \tag{31}$$

with δ related to σ by Eqn. (21) and Eqn. (8) – (20), and δ_{cg} given by Eqn. (30) above. This procedure allows us to calculate the fiber-bridging stress σ indirectly as a function of the total crack opening δ_{tot}. The flow chart of the numerical procedure for computing the bridging stress vs. crack opening displacement relationship can be found in **Fig. 9**.

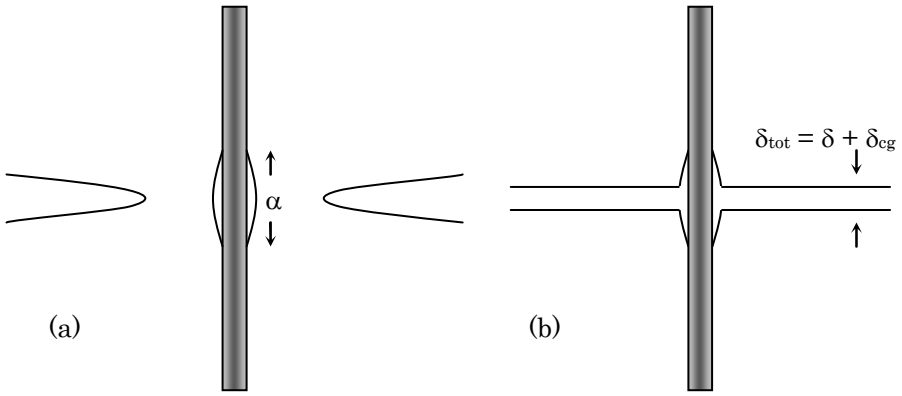

Fig. 8 Cook-Gordon effect (a) induces fiber-matrix separation due to the tensile stress in the horizontal direction associated with the elastic crack tip field of the approaching matrix crack, and (b) leads to an additional crack opening δ_{cg} due to elastic stretching of the fiber segment α in addition to the δ associated with interface frictional debonding.

4. Experimental determination of σ(δ) curve

To verify the fiber-bridging model, deformation-controlled tensile tests were conducted on notched coupon specimens to measure the σ(δ) relationship of PVA-ECC. Due to the multiple cracking nature of PVA-ECC with close crack spacing (1mm on average), it is challenging to measure the σ(δ) curve over a single crack. (A reasonably sized gauge length will cover the opening displacements of a number of subparallel microcracks, and therefore masks the true value of δ.) An alternative way to fulfill the purpose of verifying the model experimentally is to reduce the fiber content (< 2 vol.%) so that single cracking occurs. Although interfacial bond properties may change due to the reduction of fiber, the mechanisms, i.e. two way fiber pullout, Cook-Gordon effect, etc., which govern the fiber bridging behavior should nominally be unaltered. Once the validity of the fiber-bridging model is proven, the σ(δ) curve of higher fiber content can be calculated by using the corresponding micromechanics parameters.

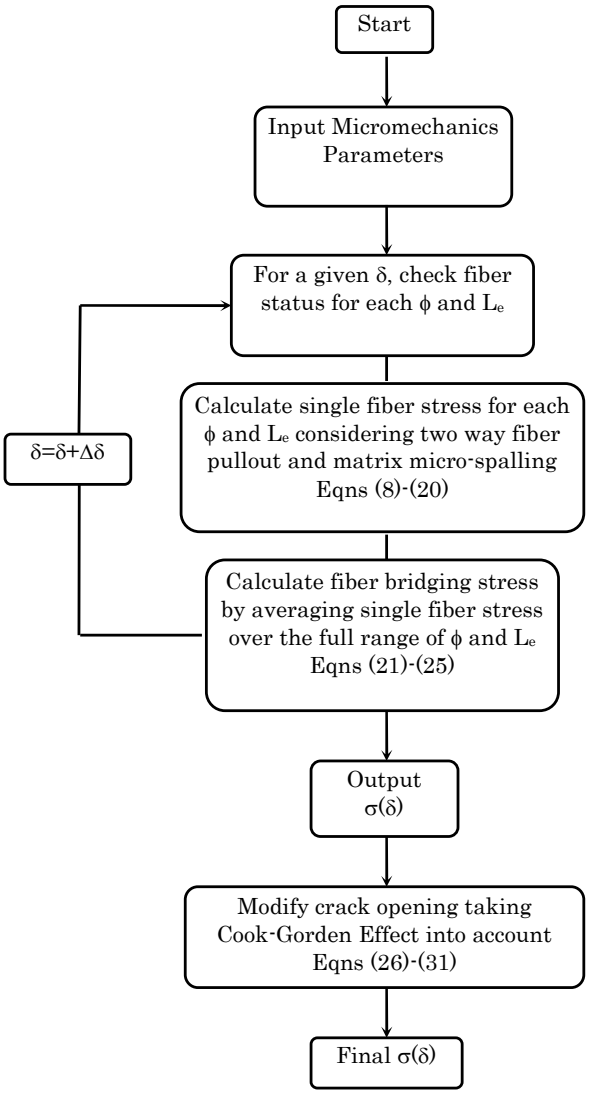

Fig. 9 Flow chart of the numerical procedure for computing σ(δ).

In this study, PVA-ECC mix 45 (M45) which is the most widely used ECC in the field was adopted for measuring the σ(δ). The mix proportion of M45 can be found in **Table 1**. The ingredients of PVA-ECC include Type I ordinary Portland cement, ASTM Class F fly ash, fine silica sand with a mean size of 110 μm, water, superplasticizer, and PVA fibers. Generally, the fiber content in PVA-ECC is 2 vol.%. In this study, M45 matrix with 0.5 vol.% and 0.1 vol.% were used in order to generate a single crack under uniaxial tensile loading. The dimensions of the PVA fiber are 12 mm in length and 39 μm in diameter on average. The nominal tensile strength of the fiber is 1600 MPa and the density of the fiber is 1300 kg/m^3. The fiber is surface-coated by oil (1.2% by weight) in order to reduce the fiber/matrix interfacial bond strength. This decision was made through ECC micromechanics material design theory and has been experimentally demonstrated from previous investigations (Li *et al*. 2002).

A Hobart mixer with 10L capacity was used in preparing the PVA-ECC mixes. Solid ingredients, including cement, fly ash, and sand, were first mixed for a couple of minutes. Water and superplasticizer were then added into the dry mix and mixed for another three minutes. The liquefied fresh mortar matrix should reach a consistent and uniform state before adding fibers. After examining the mortar matrix and making sure that there is no clump at the bottom of the mixer, PVA fibers were slowly added into the mortar matrix and mixed until all fibers are evenly distributed. The mixture was then cast into coupon molds. The specimens were demolded after 24 hours, and air cured at 50±5% RH, 23±2 ^{0}C until the age of 28 days for testing.

Notched coupon specimens with thickness 13mm, width 76mm, and height 90mm were used to conduct uniaxial tensile test at the age of 28 days. The 2mm wide circumferential notch was produced before testing by a diamond saw. Deep notches (6mm) were generated at two laterals for crack initiation and shallow notches (2mm) were produced on the front and back surfaces as crack guides (**Fig. 10**). A servohydraulic testing system was used in deformation-controlled mode to conduct the uniaxial tensile test. The loading rate used was 0.0001 mm/s to simulate a quasi-static loading condition. Aluminum plates were glued both sides at the ends of coupon specimens to facilitate gripping. Two extensometers with 5mm gauge length were attached to the laterals of the specimen and across the notches to measure the crack opening δ. The test setup is shown in **Fig. 11**. The crack opening was extracted from the total average displacement across the crack measured by the two extensometers and elastic deformation outside the crack but within the 5mm gauge length was subtracted out.

Table 1 Mix proportions of PVA-ECC (M45).

V_f (vol.%)	Cement (kg/m^3)	Fly Ash (kg/m^3)	Sand (kg/m^3)	Water (kg/m^3)	HRWR(1) (kg/m^3)	Fiber(2) (kg/m^3)	Total (kg/m^3)
2	571	685	456	332	6.8	26	2076.8
0.5	571	685	456	332	6.8	6.5	2057.3
0.1	571	685	456	332	6.8	1.3	2052.1

(1) polycarboxylate-based high range water reducer
(2) PVA fiber

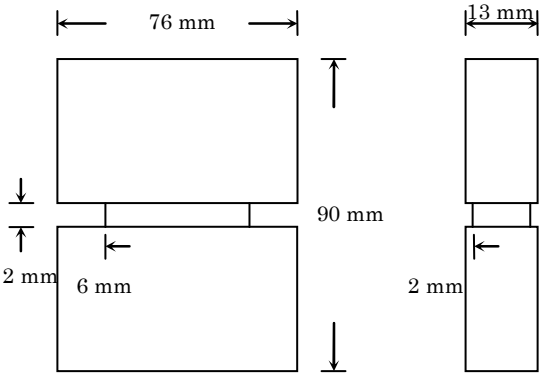

Fig. 10 Dimensions of notched coupon specimen.

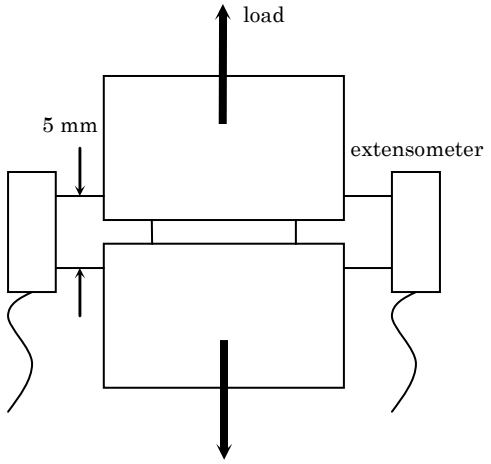

Fig. 11 Setup of uniaxial tensile test of notched specimens for experimental determination of $\sigma(\delta)$ curve.

5. Experimental validation of $\sigma(\delta)$ curve

5.1 Determination of micromechanics parameters

As can be seen, the $\sigma(\delta)$ model is related to a set of micromechanics parameters, including interface chemical bond G_d, interface frictional bond τ_0, and slip-hardening coefficient β accounting for the slip-hardening behavior during fiber pullout. In addition, snubbing coefficient f and strength reduction factor f' are introduced to account for the interaction between fiber and matrix as well as the reduction of fiber strength when pulled at an inclined angle. Besides the interfacial properties, $\sigma(\delta)$ curve is also governed by the matrix Young's modulus E_m, matrix tensile strength σ_m, matrix spalling coefficient k, fiber content V_f, fiber diameter d_f, length L_f , and Young's modulus E_f, apparent fiber strength σ_{fu}, and Cook-Gordon parameter α.

In order to calculate the analytical $\sigma(\delta)$ curve, micromechanics parameters of ECC were independently measured or deduced. **Tables 2** and **3** summarize the values of those micromechanics parameters used in the model calculation. Among them, all fiber parameters E_f, L_f, and d_f are measurable with good accuracy. The apparent fiber strength σ_{fu} and fiber strength reduction coefficient f' were measured by single fiber in-situ strength test (Kanda and Li 1998) and interface properties τ_0, G_d, and β were measured by single fiber pullout test (Redon *et al*. 2001). To measure the interfacial bond properties of ECC with different fiber volume content, M45 mortar matrix with the presence of 0.1, 0.5, and 2 vol.% PVA fibers were cast into molds and single PVA fiber was surrounded by the ECC matrix. As can be seen from **Table 3**, interfacial bond strength reduces with the increase of fiber volume content. This may be attributed to the higher air content and therefore loose pore structure in ECC when the fiber volume increases.

Wu (2001) measured f values using the early developing version of the PVA fiber that has only 0.5% oiling coating instead of 1.2% used in the current commercialized PVA REC-15 fiber, and found that the f value ranged from 0.2 to 0.8. Considering that snubbing coefficient is closely related to fiber surface frictional coefficient, which decreases significantly with increase of oiling coating content (Li *et al*. 2002), the lower end value of snubbing coefficient f = 0.2 is hence assumed in this study.

Matrix Young's modulus E_m was determined from the initial slope of the tensile stress-strain curve and the matrix tensile strength σ_m was deduced based on a wedge splitting test. The wedge splitting test (Bruehwiler and Wittmann 1990) measured the matrix fracture energy and σ_m was calculated by means of inverse analysis (Ostergaard 2003; Ostergaard *et al*. 2004). Factor k can be calibrated by measuring the spalling size. Matrix micro-spalling was collected during the uniaxial tensile test and the maximum size of matrix micro-spalling was 30 μm. Matrix spalling coefficient k

Table 2 Micromechanics parameters used as model input.

Fiber parameters				Interface parameters			Matrix parameters		
d_f (μm)	L_f (mm)	E_f (GPa)	σ_{fu} (MPa)	f	f'	α (μm)	E_m (GPa)	σ_m (MPa)	k
39	12	22	1060	0.2	0.33	78	20	5	500

Table 3 Interfacial properties of ECC.

Matrix type	τ_0 (MPa)	G_d (J/m^2)	β
0.1 vol.% PVA	1.91	1.24	0.63
0.5 vol.% PVA	1.58	1.13	0.60
2 vol.% PVA	1.31	1.08	0.58

= 500 is chosen such that the maximum spalling size calculated from Eqn. (17) (see **Fig. 6**) will not exceed the size observed in microscopic observation, i.e. 30 μm in PVA-ECC system.

To determine the Cook-Gordon parameter α, Bentur (1992) suggested $\alpha = 2d_f$ to $10d_f$ for steel fiber in neat cement paste. Li *et al*. (1993) adopted $\alpha = 15d_f$ for polypropylene fiber-reinforced concrete and found that resulting σ(δ) curve matched those of experimental data very well. For the PVA-ECC, a smaller Cook-Gordon parameter is expected due to the hydrophilic nature of PVA fiber which may introduce a stronger interface chemical bond between fiber and matrix. For lack of more precise experimental evidence, the low end suggested by Bentur, $\alpha = 2d_f$ is adopted in this study.

5.2 Comparison between model prediction and experimental results

The analytical σ(δ) curve can be calculated as long as all micromechanics parameters are determined. 2-D random fiber distribution (Eqn. (25)) was assumed in calculating the fiber-bridging model for comparison with experimental σ(δ) curves measured from coupon specimens. Because the thickness of the coupon specimen is small (13 mm) when compared with fiber length (12 mm), fiber is most likely distributed in a 2-D randomness manner. **Figure 12** shows the predicted fiber-bridging constitutive law (solid line) for M45 with V_f = 0.5 and 0.1 vol.%, respectively. In calculating these two curves, all micromechanics parameters for model input are listed in **Table 2** and **3**. Post-cracking σ(δ) curve (hollow circular dots) measured experimentally are also plotted together with the model prediction in **Fig. 12** for comparison purpose. At least 6 uniaxial tensile tests were conducted and reported in **Fig. 12** for each fiber volume.

The scattered σ(δ) curves obtained from experiments are results of material inhomogeneity, e.g. varying number of bridging fiber across crack plane for the six different specimens. Although the peak bridging stress varies in a wider range, the corresponding crack opening δ remains fairly constant. This is likely a result that with larger number of fibers, a higher load can be reached, but the crack opening will be limited by an effectively stiffer (averaged) fiber spring. This observation is also consistent with the two sets of experimental data of V_f = 0.1 and V_f = 0.5. As can be seen, the predicted σ(δ) curves which represent the mean fiber-bridging constitutive law fit well with experimental observations and the validity of this newly developed σ(δ) model is therefore confirmed.

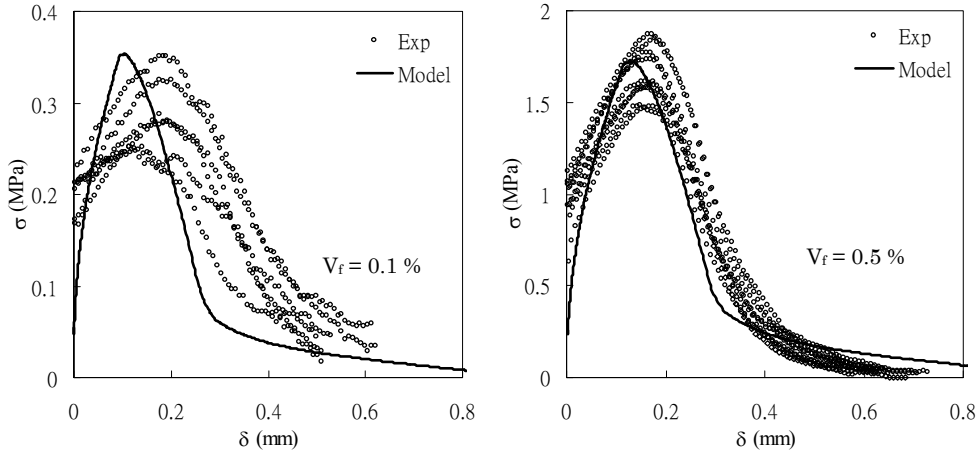

Fig. 12 Comparison of σ(δ) curves obtained from uniaxial tensile tests of notched speciemns and from model predictions of PVA-ECC for (a) V_f = 0.1 vol.% and (b) V_f = 0.5 vol.%.

6. Discussions

The middle curve in **Fig. 13(a)** displays the predicted mean $\sigma(\delta)$ curve of PVA-ECC M45 with V_f = 2 vol.% based on the same micromechanics parameters and fiber-bridging model. As can be seen, the peak bridging stress is 6.7 MPa and the corresponding crack opening is 130 μm. These values are considerably larger than the observation from composite tensile test result, in which composite ultimate tensile stress is around 5 MPa and the average crack opening is around 60 μm as depicted in **Fig. 1**.

It should be pointed out that in the composite tensile test, multiple crack surfaces are generated during the strain-hardening stage and the final failure plane is the one with the weakest bridging (lowest tensile strength capacity). If material inhomogeneity in ECC is inevitable, the observed 5 MPa ultimate tensile stress in the composite tensile test (**Fig. 1**) actually represents the lowest peak fiber-bridging stress. This observed value (5 MPa) is 25% less than the calculated peak bridging stress (6.7 MPa) and is likely attributed to varying number of bridging fiber from one crack plane to another. To simulate this variation, $\sigma(\delta)$ curves with V_f = 1.5 vol.% (25% less) and 2.5 vol.% (25% more) were calculated using the same set of micromechanics parameters as 2 vol.% except the fiber volume was changed as the lower and higher bonds of bridging, respectively. These three curves represent the variation of $\sigma(\delta)$ curve in PVA-ECC M45, among the multiple crack planes.

Following the discussion above, the weakest fiber-bridging $\sigma(\delta)$ curve is expected to dominate the composite tensile behavior. Damage localization in ECC occurs as soon as the weakest bridging plane reaches its peak bridging stress (5 MPa for M45). **Figure 13(b)** displays a magnified view of **Fig. 13(a)**. As can be seen, crack opening δ for each $\sigma(\delta)$ curve at σ = 5 MPa varies from 37 μm to 133 μm with a mean of 62 μm. This predicted mean crack opening is remarkably consistent with the average crack opening observed from the composite uniaxial tensile test (**Fig. 1**).

To evaluate contributions to the σ-δ of each of the three newly introduced mechanisms, theoretical $\sigma(\delta)$ curves calculated by various models are presented in **Fig. 14**. When only one-way pullout is considered, e.g. previous simplified model by Lin *et al*. (1999), the predicted peak bridging stress and corresponding crack opening are 6.2 MPa and 93 μm respectively. If two-way pullout is accounted for but without considerations of spalling and Cook-Gordon effects, a peak stress 6.3 MPa is attained at crack opening of 130 μm. When both two-way pullout and matrix spalling are considered but without consideration of Cook-Gordon effect, the model predicts a peak stress 6.7 MPa at 131 μm. If all three newly introduced mechanisms are accounted for, the predicted peak bridging stress and corresponding crack opening are 6.7 MPa and 133 μm respectively. A direct comparison between these four curves reveals that two-way pullout is most responsible for overcoming the underprediction of crack opening in PVA-ECC system using the previous model version. The contribution of matrix spalling to crack opening is rather small. Matrix spalling, which effectively reduces the inclination angle for individual fibers, delays fibers to rupture, and therefore raises the peak bridging stress. In contrast, if there is no matrix spalling, fiber with large inclination angle will rupture at much earlier stage due to higher fiber strength reduction. Cook-Gordon effect does not show remarkable impact on crack opening due to the assumption of small Cook-Gordon parameter $\alpha = 2d_f$ which is likely the case for the hydrophilic PVA fiber. However, the Cook-Gordon effect may play an important role in other fiber-reinforced ECC systems, such as polyethylene (PE) and polypropylene (PP) fibers, in which the fiber/matrix interface chemical bond is close to zero and a larger Cook-Gordon parameter α is expected due to the hydrophobic nature of PE and PP fibers.

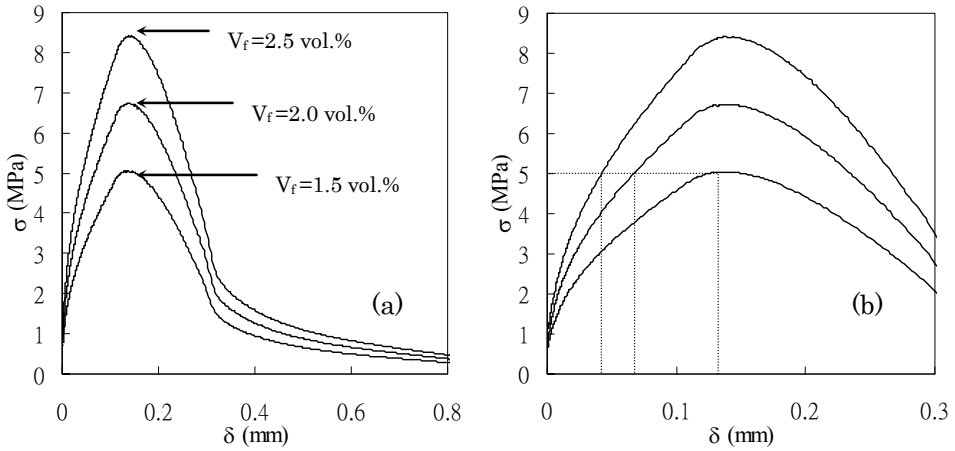

Fig. 13 (a) Predicted $\sigma(\delta)$ curve of PVA-ECC M45 with V_f = 2 vol.% (full span), and (b) magnified view of (a) (δ = 0 ~ 0.3 mm). The three curves in each plot are generated assuming fiber volume variation due to processing of ECC composites, see text.

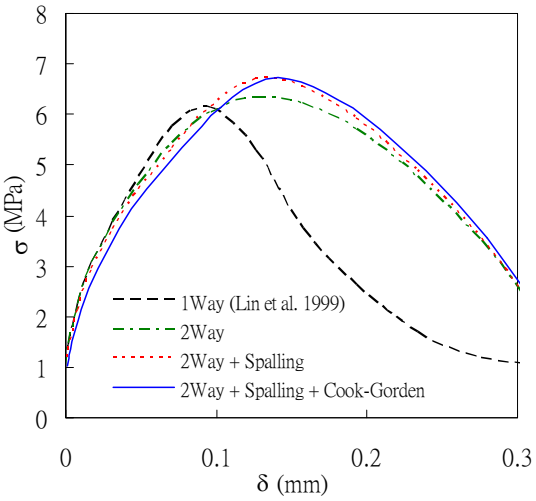

Fig. 14 Theoretical bridging stress vs. crack opening relation of PVA-ECC calculated by various models.

7. Conclusions

An analytical fiber-bridging model was developed and experimentally verified in this study. This model improves over an earlier version by including three new mechanisms of fiber/matrix interactions in order to accurately predict the σ(δ) curve of ECC in general, and improve accuracy of crack opening prediction in particular. For the PVA-ECC system, it was found that two-way fiber pullout mechanism is most responsible for enhancing the correction prediction of the crack opening. The predicted crack opening based on this model can reproduce those in PVA-ECC composite tests when variability in bridging fiber volume from one crack plane to another is recognized.

Although this model is suitable especially for the PVA-ECC system, it is likely applicable to other fiber systems as long as the appropriate governing fiber/matrix interaction mechanisms are captured. This revised fiber-bridging model will greatly improve ECC micromechanics-based material design theory in terms of crack width (which strongly governs structural durability) and composite tensile ductility (which strongly governs structural load carrying capacity and deformability).

References

Bentur, A. (1992). Personal communication.

Bruehwiler, E. and Wittmann, F. H. (1990). "The wedge splitting test, A new method of performing stable fracture mechanics test." *Engineering Fracture Mechanics,* 35(1-3), 117-125.

Fischer, G. and Li, V. C. (2002). "Effect of matrix ductility on deformation behavior of steel reinforced ECC flexural members under reversed cyclic loading conditions." *ACI Structural Journal,* 99(6), 781-790.

Fischer, G., Wang, S. and Li, V. C. (2003). "Design of engineered cementitious composites (ECC) for processing and workability requirements." in Proc., *BMC-7*, Warsaw, Poland, Eds. A.M. Brandt, V.C. Li, and I.H. Marshall, pp. 29-36.

Fukuyama, H., Matsuzaki, Y., Nakano, K. and Sato, Y. (1999). "Structural performance of beam elements with PVA-ECC." In *Proc. of High Performance Fiber Reinforced Cement Composites 3* (*HPFRCC 3*), Reinhardt and A. Naaman, eds., pp. 531-542. Chapman & Hull.

Kanda, T. and Li, V. C. (1998). "Interface property and apparent strength of a high strength hydrophilic fiber in cement matrix." *ASCE Journal of Materials in Civil Engineering,* 10(1), 5-13.

Kong, H. J., Bike, S. and Li, V. C. (2003). "Constitutive rheological control to develop a self-consolidating engineered cementitious composite reinforced with hydrophilic poly(vinyl alcohol) fibers." *Journal of Cement and Concrete Composites,* 25(3), 333-341.

Kunieda, M. and Rokugo, K. (2006). "Recent progress on HPFRCC in Japan." *Journal of Advanced Concrete Technology,* 4 (1), 19-33.

Lepech, M. and Li, V. C. (2005a). "Durability and long term performance of engineered cementitious composites." In G. Fisher, and V. C. Li Eds. *Proceedings of International RELIM Workshop on HPFRCC in Structural Applications*, Honolulu, Hawaii, 165-174.

Lepech, M. and Li, V. C. (2005b). "Water permeability of cracked cementitious composites." In *Proceeding of Eleventh International Conference on Fracture*, Turin, Italy, CD-Paper 4539.

Li, V. C. (1997). "Engineered cementitious composites - Tailored composites through micromechanical modeling." In N. Banthia, A. Bentur, and A. Mufti Eds. *Fiber Reinforced Concrete: Present and the Future*. Montreal, Canadian Society for Civil Engineering, 64-97.

Li, V. C., Mishra, D. K., Naaman, A. E., Wight, J. K., LaFave, J. M., Wu, H. C. and Inada, Y. (1994). "On the shear behavior of engineered cementitious composites." *J. of Advanced Cement Based Materials*, 1(3), 142-149.

Li, V. C. and Stang, H. (2004). "Elevating FRC material ductility to infrastructure durability." In *Proceedings of BEFIB 2004*, Lake Como, Italy, 171-186.

Li, V. C. and Wang, S. (2002). "Flexural behavior of GFRP reinforced engineered cementitious composites beams." *ACI Materials Journal,* 99(1), 11-21.

Li, V. C., Lepech, M. and Li, M. (2005). Field demonstration of durable link slabs for jointless bridge decks based on strain-hardening cementitious composites, Michigan DOT report.

Li, V. C., Stang, H. and Krenchel, H. (1993). "Micromechanics of crack bridging in fibre-reinforced concrete." *Materials and Structures,* (26), 486-494.

Li, V. C., Wang, S. and Wu, C. (2001). "Tensile strain-hardening behavior of PVA-ECC." *ACI Materials Journal,* 98(6), 483-492.

Li, V. C., Wu, C., Wang, S., Ogawa, A. and Saito, T. (2002). "Interface tailoring for strain-hardening PVA-ECC." *ACI Materials Journal,* 99(5), 463-472.

Lin, Z. and Li, V. C. (1997). "Crack bridging in fber reinforced cementitious composites with slip-hardening interfaces." *Journal of Mechanics and Physics of Solids,* 45(5), 763-787.

Lin, Z., Kanda, T. and Li, V. C. (1999). "On interface property characterization and performance of fiber-reinforced cementitious composites." *Journal of Concrete Science and Engineering,* (1), 173-184.

Maalej, M., Hashida, T. and Li, V. C. (1995). "Effect of fiber volume fraction on the off-crack plane energy in strain-hardening engineered cementitious composites." *Journal of American Ceramics Society,* 78(12), 3369-3375.

Marshall, D. B. and Cox, B. N. (1988). "A J-integral method for calculating steady-state matrix cracking stresses in composites." *Mechanics of Materials,* (8), 127-133.

Michigan_DOT (2005). "Bridge decks going jointless: Cementitious composites improve durability of link slabs." *Construction and Technology Research Record,* (100), 1-4.

Miyazato, S. and Hiraishi, Y. (2005). "Transport properties and steel corrosion in ductile fiber reinforced cement composites." In *Proc. ICF 11*, Torino, Italy,

Morton, L. and Groves, G. W. (1976). "The effect of met al wires on the fracture of a brittle mtrix composite." *Journal of Material Science,* (11), 617-622.

Ostergaard, L. (2003). "*Early-age fracture mechanics and cracking of concrete - Experiments and modeling*." Thesis (Ph.D.), Technical University of Denmark.

Ostergaard, L., Lange, D. and Stang, H. (2004). "Early-age stress-crack opening relationships for high performance concrete." *Cement and Concrete Composites,* 26(5), 563-572.

Redon, C., Li, V. C., Wu, C., Hoshiro, H., Saito, T. and Ogawa, A. (2001). "Measuring and modifying interface properties of PVA fibers in ECC matrix." *ASCE Journal of Materials in Civil Engineering,* 13(6), 399-406.

Sahmaran, M., Li, M. and Li, V. C. (2007). "Transport properties of engineered cementitious composites under chloride exposure." *ACI Materials Journal,* 104(6), 303-310.

Wang, S. and Li, V. C. (2006). "High-early-strength engineered cementitious composites." *ACI Materials Journal,* 103(2), 97-105.

Wang, Y., Backer, S. and Li, V. C. (1990). "A statistical tensile model of fiber reinforced cementitious composites." *Journal of Composites,* 20(3), 265-274.

Wang, Y., Li, V. C. and Backer, S. (1988). "Modeling of fiber pll-out from a cement matrix." *Int'l J. of Cement Composites and Lightweight Concrete,* 10(3), 143-149.

Wu, C. (2001). "*Micromechanical tailoring of PVA-ECC for structural application*." Thesis (Ph.D.), University of Michigan.

Yang, Y., Lepech, M. and Li, V. C. (2005). "Self-healing of ECC under cyclic wetting and drying." In *Proceedings of Int'l Workshop on durability of reinforced concrete under combined mechanical and climatic loads*, Qingdao, China, 231-242.

Zhang, J., Maalej, M., Quek, S. T. and Teo, Y. Y. (2005). "Drop weight impact on hybrid-fiber ECC blast/shelter panels." In *Proceedings of the 3rd International Conference on Construction Materials: Performance, Innovations and Structural Implications* Vancouver, Canada, CD paper.